AIMS Mathematics, 7(11): 19902–19921.
DOI: 10.3934/math.20221090
Received: 20 June 2022
Revised: 08 August 2022
Accepted: 16 August 2022
Published: 08 September 2022

http://www.aimspress.com/journal/Math

Research article

Sensitivity analysis and design optimization of 3T rotating thermoelastic structures using IGBEM

Mohamed Abdelsabour Fahmy[1,2,*], Mohammed O. Alsulami[3] and Ahmed E. Abouelregal[4,5]

[1] Adham University College, Umm Al-Qura University, Adham 28653, Makkah, Saudi Arabia
[2] Faculty of Computers and Informatics, Suez Canal University, New Campus, 41522 Ismailia, Egypt
[3] Department of Mathematical Sciences, Faculty of Applied Sciences Umm Al-Qura University, Makkah 24381, Saudi Arabia
[4] Department of Mathematics, College of Science and Arts, Jouf University, Al-Qurayyat 72388, Saudi Arabia
[5] Department of Mathematics, Faculty of Science, Mansoura University, Mansoura 35516, Egypt

* **Correspondence:** Email: maselim@uqu.edu.sa; Tel: 00966537930306.

Abstract: In this study, the isogeometric boundary element method (IGBEM) based on non-uniform rational basis spline (NURBS) is used to perform shape design sensitivity and optimization of rotating three-temperature (3T) thermoelastic structures. During the optimization process, the shape design sensitivity within the IGBEM formulation was derived to include precise geometries and greater continuities. It was found through the application of the IGBEM that the shape design velocity has a significant effect on accuracy of the obtained shape design sensitivity. As a result, the developed shape design sensitivity analysis (SDSA) technique based on the considered IGBEM formulation outperforms the computational solution based on the traditional SDSA method. The isogeometric shape sensitivity and optimal design for a complicated three-temperature thermoelastic problem in rotating structures are investigated. The impact of rotation on the thermal stress sensitivity, optimal three-temperature, optimal displacement and optimal three temperature thermal stress distributions are established. It is shown that the SDSA derived using IGBEM is efficient and applicable for most three-temperature thermoelastic optimization problems.

Keywords: sensitivity; optimization; three-temperature; rotation; thermoelastic structures; isogeometric boundary element method
Mathematics Subject Classification: 35Qxx, 65Zxx

1. Introduction

Various aspects of engineering are coupled or interconnected with each other, including structural response, changes of temperature, fields of electromagnetic, and interactions of fluid-structure. In thermoelasticity, the heat conductivity of an elastic body is not affected by its deformation because the statement that the distortion of an elastic body does not change the heat conductivity is true. Extensive thermoplastic design efforts are common in plant design and nuclear industries, where thermomechanical coupling by chemical and atomic responses has a significant impact on practical devise analyses. Another demand for coupled thermoelasticity is practically evaluated resources [1], of which nonhomogeneous thermal and mechanical properties are depicted by the arrange role, i.e., design parameters, to oppose thermal stacking and maintain structural intensity.

The combined shape plan and execution evaluation of mechanical components has been a focal point in CAD and CAE businesses to get the best and optimized designing arrangement, and the recently created isogeometric analysis (IGA) system by Hughes et al. [2] encourages consistent joining between building investigation and geometric representation by utilizing the same non-uniform rational basis spline (NURBS) premise capacities to parameterize the arrangement space. In areas where modern geometry representations are required, such as shell investigation [3,4], fluid-structure interaction [5,6], and shape plan optimization [6,7], isogeometric approaches have been used. The isogeometric method was used to investigate thermoelastic behavior, the thermomechanical gun dealings problem [8], and fabric dispersion of practically evaluated structures [9,10].

The boundary element strategy was created to decipher the supervising partial differential conditions as the boundary indispensably conditions of the relocation and footing areas over the boundary [11,12]. Several complicated thermoelastic problems have been established in the literature to solve such problems, numerical techniques, such as the boundary element method (BEM), have been investigated in the context of micropolar-thermoelasticity [13], carbon nanotube fiber reinforced composites [14], micropolar piezothermoelasticity [15], Micropolar Magne-to-thermoviscoelasticity [16], and Magneto-thermoviscoelasticity [17]. Fahmy also introduced new boundary element models for bioheat problems [18], Thermoelastic problems of Metal and Alloy Discs with Holes [19], Wave Propagation Problems of Anisotropic Fiber-Reinforced Plates [20], size-dependent thermopiezoelectric problems [21], three-temperature problems [22], and photothermal problems [23].

The use of IGBEM in shape optimization [24] may be a natural extension of IGA-based shape optimization considerations of References [6,25], in which precise geometric data is used and shape plan factors are streamlined. Furthermore, IGBEM-based optimization has greater ideal shape plan flexibility than IGA-based optimization. [26]. Since the mid-1980s, affectability studies and plan optimization of thermally coupled frameworks have been carried out [27]. Dems and Mroz [28] performed variational thermoelasticity sensitivity analysis using sizing and shape variables. Tortorelli

and Subramani [29] used the adjoint approach to analyze sensitivity for a coupled constitutive model. Optimization of shape and topology for problems of thermoelastic was introduced by Hou, Sheen [30] and Li, Steven [31]. The integral equation of boundary was used by Lee and Kwak [32] to examine optimization of shape design. The plan optimization of fabric dispersion for thermally stacked FGMs has been broadly considered owing to the design element of FGMs. Fang et al. [33] studied isogeometric boundary element analysis for two-dimensional thermoelasticity with variable temperature. Lieu and Lee [34] used the isogeometric approach to optimize practically reviewed structures while accounting for thermoelasticity. An et al. [35] investigated the implementation of isogeometric boundary element method for 2-D steady heat transfer analysis.

In this paper, a new isogeometric boundary element method (IGBEM) based on non-uniform rational basis spline (NURBS) is developed to perform shape design sensitivity and optimization of rotating three-temperature (3T) thermoelastic structures. The isogeometric shape sensitivity and optimal design for a complicated three-temperature thermoelastic problem in rotating structures are investigated. The shape design sensitivity analysis (SDSA) derived using IGBEM is shown to be efficient and applicable to most three-temperature thermoelastic optimization problems. Using the IGBEM in the design of thermos-mechanical structures allow for accurate thermal boundary representation as well as simple design parameterization for optimization. We primarily focus on developing the continuum-based shape affectability condition of coupled thermoelastic conditions and demonstrating the optimization results of viable appropriateness utilizing the inferred equation, utilizing these benefits within the optimization strategy. Derivation and verification of thermoelastic structure sensitivity using a continuum-based coupled shape design within the IGBEM was described, the derived sensitivity formula was used to solve the coupled thermos-mechanical optimization problem. The IGBEM approach based on NURBS was discussed. The affectability of an isogeometric shape plan is then determined using a boundary fundamental condition for considered thermoelastic problem. Rotation influences on the thermal stress σ_{11} sensitivity, optimal $3T$ distribution θ, optimal displacement u, and optimal $3T$ thermal stress σ_{11} are presented graphically. Numerical results demonstrate the validity, accuracy, and efficiency of the proposed technique.

2. NURBS basis function

The response field in the IGBEM is approximated using the unchanged premise functions that are utilized to describe the geometry within CAD. Due to the employ of NURBS premise functions, which are based on B-splines, the IGBEM has various focal points over the usual BEM, including geometric precision and ease of refinement. Let a one-dimensional tie vector Ξ which contains a collection of ties ξ_i can be written as

$$\Xi = \{\xi_1, \xi_2, \cdots, \xi_{n+p+1}\}, \tag{1}$$

where n and p are points of control number, and the function of basis order, respectively.

A basis function of NURBS $R_i^p(\xi)$ is defined as $R_i^p(\xi) = \frac{N_i^p(\xi)w_i}{\sum_{j=1}^n N_j^p(\xi)w_j}$.

The definition of $N_i^0(\xi)$ functions is, recursively

$$N_i^0(\xi) = \begin{cases} 1 & \text{if } \xi_i \le \xi < \xi_{i+1}, \ (p = 0), \\ 0 & \text{otherwise} \end{cases} \tag{2}$$

and

$$N_i^p(\xi) = \frac{\xi - \xi_i}{\xi_{i+p} - \xi_i} N_i^{p-1}(\xi) + \frac{\xi_{i+p+1} - \xi}{\xi_{i+p+1} - \xi_{i+1}} N_{i+1}^{p-1}(\xi), \ (p = 1,2,3, \dots). \tag{3}$$

In general, the IGBEM, which employs higher-order premise functions, yields higher levels of normality than the standard BEM. A NURBS bend is characterized by the summation of n sets of the p-th-order NURBS premise function $\mathrm{R}_l^p(\xi)$ multiplied by the matching control point $\mathbf{B}_i$ [36–38]. Over each specific knot, the developed NURBS basis functions have relative invariance and (p−1) incessant differentiability, where p is the arrangement of the fundamental polynomial. If the knots are repeated k-times, the continuity of NURBS basis functions decreases by k.

3. BEM solution of three temperature field

The three-temperature radiation heat transfer equations can be expressed as

$$C_{ve} \frac{\partial \theta_e(r,\tau)}{\partial \tau} - \frac{1}{\rho} \nabla[\mathbb{K}_e \nabla \theta_e(r,\tau)] = -\mathbb{W}_{ei}(\theta_e - \theta_i) - \mathbb{W}_{er}(\theta_e - \theta_r), \tag{4}$$

$$C_{vi} \frac{\partial \theta_i(r,\tau)}{\partial \tau} - \frac{1}{\rho} \nabla[\mathbb{K}_i \nabla \theta_i(r,\tau)] = \mathbb{W}_{ei}(\theta_e - \theta_i), \tag{5}$$

$$C_{vr} \frac{\partial \theta_r(r,\tau)}{\partial \tau} - \frac{1}{\rho} \nabla[\mathbb{K}_r \nabla \theta_r(r,\tau)] = \mathbb{W}_{er}(\theta_e - \theta_r). \tag{6}$$

In which

$$C_{v\alpha} = \begin{cases} c_e & \alpha = e \\ c_i & \alpha = i \\ c_r \theta_r^3 & \alpha = r \end{cases} \text{ and } \mathbb{K}_\alpha = \begin{cases} \mathbb{A}_e \theta_e^{5/2} & \alpha = e \\ \mathbb{A}_i \theta_i^{5/2} & \alpha = i \\ \mathbb{A}_r \theta_r^{3+\mathbb{B}} & \alpha = r \end{cases},$$

where ρ is the material density, $\theta = \theta_e + \theta_i + \theta_r$, is the total temperature, $\mathbb{W}_{ei} = \rho \mathbb{A}_{ei} \theta_e^{-2/3}$ and $\mathbb{W}_{er} = \rho \mathbb{A}_{er} \theta_e^{-1/2}$ are energy exchanging coefficients, and c_α $(\alpha = e, i, r)$ are constants.

According to Fahmy et al. [17], the three-temperature heat conduction Eqs (4)–(6) may be written as

$$\nabla[\mathbb{K}_\alpha \nabla \theta_\alpha(r,\tau)] + \overline{\mathbb{W}}(r,\tau) = c_\alpha \rho \delta_1 \frac{\partial \theta_\alpha(r,\tau)}{\partial \tau}, \tag{7}$$

where

$$\overline{\mathbb{W}}(r,\tau) = \begin{cases} -\rho \mathbb{W}_{ei}(\theta_e - \theta_i) - \rho \mathbb{W}_{er}(\theta_e - \theta_r), \alpha = e, \delta_1 = 1 \\ \rho \mathbb{W}_{ei}(\theta_e - \theta_i), \qquad \alpha = i, \delta_1 = 1 \\ \rho \mathbb{W}_{er}(\theta_e - \theta_r), \qquad \alpha = r, \delta_1 = T_r^3 \end{cases}. \tag{8}$$

The unit mass total energy is given by

$$P = P_e + P_i + P_r, P_e = c_e \theta_e, P_i = c_i \theta_i, P_r = \frac{1}{4} c_r \theta_r^4. \tag{9}$$

The considered conditions can be composed as

$$\theta_\alpha(x,y,0) = \theta_\alpha^0(x,y) = g_1(x,\tau). \tag{10}$$

$$\mathbb{K}_\alpha \frac{\partial \theta_\alpha}{\partial n}\Big|_{\Gamma_1} = 0, \alpha = e,i,\theta_r|_{\Gamma_1} = g_2(x,\tau). \tag{11}$$

$$\mathbb{K}_\alpha \frac{\partial \theta_\alpha}{\partial n}\Big|_{\Gamma_2} = 0, \alpha = e,i,r. \tag{12}$$

Using the fundamental solution which satisfies the following equation

$$D\nabla^2\theta_\alpha + \frac{\partial \theta_\alpha^*}{\partial n} = -\delta(r-p_i)\delta(\tau - r),\ D = \frac{\mathbb{K}_\alpha}{\rho c}, \tag{13}$$

where p_i are singular points.

The transient heat conduction can be written as

$$C\theta_\alpha = \frac{D}{\mathbb{K}_\alpha}\int_O^\tau \int_S \left[\theta_\alpha q^* - \theta_\alpha^* q\right] dSd\tau + \frac{D}{\mathbb{K}_\alpha}\int_O^\tau \int_R\ b\,\theta_\alpha^*\, dRd\tau + \int_R \theta_\alpha^i \theta_\alpha^*\big|_{\tau=0}\, dR, \tag{14}$$

which can be expressed as follows

$$C\theta_\alpha = \int_S \left[\theta_\alpha q^* - \theta_\alpha^* q\right] dS - \int_R \frac{\mathbb{K}_\alpha}{D}\frac{\partial \theta_\alpha^*}{\partial \tau}\theta_\alpha dR. \tag{15}$$

Let us assume that the time temperature derivative may be approximated as

$$\frac{\partial \theta_\alpha}{\partial \tau} \cong \sum_{j=1}^N f^j(r)^j a^j(\tau), \tag{16}$$

where $f^j(r)$ are known functions and $a^j(\tau)$ are unknown coefficients.

Suppose that $\hat{\theta}_\alpha^j$ is a solution of

$$\nabla^2\hat{\theta}_\alpha^j = f^j. \tag{17}$$

Thus, Eq (15) can be written as

$$C\theta = \int_S \left[\theta_\alpha q^* - \theta_\alpha^* q\right] dS + \sum_{j=1}^N a^j(\tau) D^{-1}\left(C\hat{\theta}_\alpha^j - \int_S \left[\theta_\alpha^j q^* - \hat{q}^j\theta_\alpha^*\right] dS\right), \tag{18}$$

where

$$\hat{q}^j = -\mathbb{K}_\alpha \frac{\partial \hat{\theta}_\alpha^j}{\partial n} \tag{19}$$

and

$$a^j(\tau) = \sum_{i=1}^N f_{ji}^{-1}\frac{\partial \theta(r_i,\tau)}{\partial \tau} \tag{20}$$

where f_{ji}^{-1} are defined as [33].

$$\{F\}_{ji} = f^j(r_i). \tag{21}$$

From Eqs (18) and (20), we obtain

$$C\dot{\theta}_\alpha + H\theta_\alpha = GQ, \tag{22}$$

where

$$C = -\left[H\hat{\theta}_\alpha - G\hat{Q}\right]F^{-1}D^{-1}, \tag{23}$$

with

$$\left\{\hat{\theta}\right\}_{ij} = \hat{\theta}^j(x_i), \tag{24}$$

$$\left\{\hat{Q}\right\}_{ij} = \hat{q}^j(x_i). \tag{25}$$

Now, we interpolate the functions θ_α and q as

$$\theta_\alpha = (1-T)\theta_\alpha^m + T\theta_\alpha^{m+1}, \tag{26}$$

$$q = (1-T)q^m + Tq^{m+1}, \tag{27}$$

where $0 \le T = \frac{\tau-\tau^m}{\tau^{m+1}-\tau^m} \le 1$.

Differentiation of (26) yields

$$\dot{\theta}_\alpha = \frac{d\theta_\alpha}{dT}\frac{dT}{d\tau} = \frac{\theta_\alpha^{m+1}-\theta_\alpha^m}{\tau^{m+1}-\tau^m} = \frac{\theta_\alpha^{m+1}-\theta_\alpha^m}{\Delta\tau^m}. \tag{28}$$

Substitution of Eqs (31)–(33) into Eq (27), yields

$$\left(\frac{C}{\Delta\tau^m} + TH\right)\theta_\alpha^{m+1} - TGQ^{m+1} = \left(\frac{C}{\Delta\tau^m} - (1-T)H\right)\theta_\alpha^m + (1-T)GQ^m, \tag{29}$$

which can be written as

$$\mathbb{a}\mathrm{X} = \mathbb{b}. \tag{30}$$

Because the successive over-relaxation (SOR) method requires less memory than the Jacobi and Gauss-Seidel iterative methods [38], it was efficiently implemented to solve the resulting linear algebraic systems.

4. BEM solution of displacement field

Figure 1 illustrates the case of considered model in an open domain Ω that is bounded by a closed surface Γ, The boundaries existing of the mechanical and thermal are independently on Ω. Temperature Γ_θ^0, flux Γ_θ^1, and convection Γ_θ^2. boundaries are thermal boundaries. Displacement Γ_D and traction Γ_N. boundaries are mechanical boundaries. In addition, the boundaries are independent.

The properties of considered model material in domain Ω are supposed to be isotropic and elastic, as well as temperature independent.

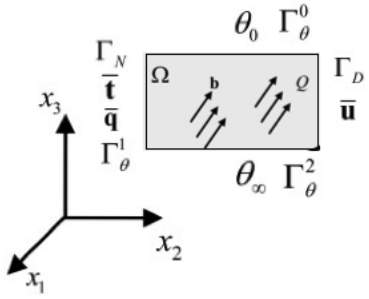

Figure 1. Boundary problem of thermoelasticity.

The internal heat production rate Q and the next thermal boundary conditions apply to the body: A endorsed temperature θ_0 on Γ_θ^0, a endorsed heat flux $\bar{\mathbf{q}}$ on Γ_θ^1, and an surrounding temperature θ_∞ on the convection boundary Γ_θ^2. In addition, a body power strength $\mathbf{b}$ as well as the next mechanical boundary conditions apply to the body: A endorsed displacement $\bar{\mathbf{u}}$ on Γ_D and a endorsed traction $\bar{\mathbf{t}}$ on Γ_N.

The equilibrium equation is

$$\sigma_{ij,j} + b_i = 0 \text{ in } \Omega. \tag{31}$$

The boundary conditions are

$$u_i = \bar{u}_i \, on \, \Gamma_D, \tag{32}$$

and

$$t_i = \sigma_{ij} n_j = \bar{t}_i \text{ on } \Gamma_N. \tag{33}$$

Suppose that the stress-strain relation in thermoelasticity is weakly coupled and is stated as

$$\sigma_{ij} = 2\mu \left[\varepsilon_{ij} + \frac{1}{1-2v} \varepsilon_{kk} \delta_{ij} \right] - \frac{E}{1-2v} \alpha \theta \delta_{ij}. \tag{34}$$

With θ $(\theta = \theta_e + \theta_i + \theta_r)$ is the total temperature calculated from section 3, μ, ε_{ij}, δ_{ij}, v, E and α are shear modulus, strain tensor, Kronecker delta, Poisson's ratio, Young's modulus, and thermal expansion coefficient, respectively.

The solution $\mathbf{u}^*$ should satisfy the following:

$$\sigma_{ij,j}(\mathbf{u}^*) = -\delta(\mathbf{x} - \hat{\mathbf{x}}) e_i, \tag{35}$$

$$u_i^* = U_{ij} e_j, \tag{36}$$

$$\sigma_{ij}(\mathbf{u}^*) n_j = T_{ij} e_i, \tag{37}$$

here e_i represents a unit vector.

$$U_{ij}(\mathbf{x}, \hat{\mathbf{x}}) = \frac{1}{8\pi\mu(1-v)} \left[(3-4v) \ln \frac{1}{r} \delta_{ij} + r_{,i} r_{,j} \right], \tag{38}$$

and

$$T_{ij}(\mathbf{x},\hat{\mathbf{x}}) = -\frac{1}{4\pi(1-\nu)r}\left[\frac{\partial r}{\partial n}\left[(1-2\nu)\delta_{ij}+2r_{,i}r_j\right]+(1-2\nu)\left(n_i r_{,j}-n_j r_{,i}\right)\right], \tag{39}$$

with $r = \| \hat{\boldsymbol{x}} - \boldsymbol{x} \|$ is the distance function. The mechanical problem boundary integral equations can be written accordingly using the fundamental solution:

$$\begin{aligned} &u_j(\hat{\mathbf{x}}) + \int_\Gamma T_{ij}(\mathbf{x},\hat{\mathbf{x}})u_i d\Gamma \\ &= \int_\Gamma t_i U_{ij}(\mathbf{x},\hat{\mathbf{x}})d\Gamma + \frac{E\alpha}{1-2\nu}\int_\Omega U_{ij,i}(\mathbf{x},\hat{\mathbf{x}})\theta d\Omega + \int_\Omega b_i U_{ij} d\Omega. \end{aligned} \tag{40}$$

Using a Galerkin vector, Eq (40) can be rewritten as

$$\begin{aligned} &u_j(\hat{\mathbf{x}}) + \int_\Gamma T_{ij}(\mathbf{x},\hat{\mathbf{x}})u_i d\Gamma - \int_\Gamma \bar{P}_j(\mathbf{x},\hat{\mathbf{x}})\theta(\mathbf{x})d\Gamma \\ &= \int_\Gamma t_i U_{ij}(\mathbf{x},\hat{\mathbf{x}})d\Gamma + \int_\Gamma q_n \bar{Q}_j(\mathbf{x},\hat{\mathbf{x}})d\Gamma + \int_\Omega b_i U_{ij} d\Omega. \end{aligned} \tag{41}$$

A two-dimensional problem has the following fundamental solutions:

$$\bar{P}_i(\mathbf{x},\hat{\mathbf{x}}) = \frac{\alpha(1+\nu)}{4\pi(1-\nu)}\left\{\left[\ln\left(\frac{1}{r}-\frac{1}{2}\right)n_i - r_{,i}r_{,k}n_k\right]\right\} \tag{42}$$

and

$$\bar{Q}_i(\mathbf{x},\hat{\mathbf{x}}) = -\frac{(1+\nu)}{4\pi k(1-\nu)}\alpha r r_{,i}\left[\ln\left(\frac{1}{r}\right)-\frac{1}{2}\right]. \tag{43}$$

Integral characters [39] for fundamental solutions of the singular integral at were utilized, as well as the transformation method. In Eq (41), we can write the regularized boundary integral equations as follows:

$$\begin{aligned} &\int_\Gamma T_{ij}(\mathbf{x},\hat{\mathbf{x}})\{u_i(\mathbf{x}) - u_i(\hat{\mathbf{x}})\}d\Gamma - \int_\Gamma \bar{P}_j(\mathbf{x},\hat{\mathbf{x}})\theta(\mathbf{x})d\Gamma \\ &= \int_\Gamma t_i U_{ij}(\mathbf{x},\hat{\mathbf{x}})d\Gamma + \int_\Gamma q_n \bar{Q}_j(\mathbf{x},\hat{\mathbf{x}})d\Gamma + \int_\Omega b_i U_{ij} d\Omega. \end{aligned} \tag{44}$$

Isoparametric mapping, based on pth order NURBS basis functions, is a technique for expressing geometric point and response as follows:

$$q_n(\Xi) = \sum_{I=1}^{CPT} R_I^p(\Xi) w_I, \tag{45}$$

$$\mathbf{u}(\xi) = \sum_{I=1}^{CP} R_I^p(\xi)\mathbf{y}_I \tag{46}$$

and

$$\mathbf{t}(\xi) = \sum_{I=1}^{CPT} R_I^p(\xi)\mathbf{z}_{\boldsymbol{I}}, \tag{47}$$

with $\mathbf{v}_I$ is a coefficient of temperature, w_I is a coefficient of normal flux, $\mathbf{y}_I$ is a coefficient of displacement, $\mathbf{z}_{\boldsymbol{I}}$ is a coefficient of traction, CP is control points number, and CPT is normal fluxes number. Finally, for simplicity, Eqs (27) and (28) are discretized in a form of matrix using NURBS based basis functions.

$$\mathbf{H}_I^N \mathbf{y}_I - \bar{H}_I^\theta \mathbf{H}_I^\theta \mathbf{v}_I = \mathbf{G}_I^D \mathbf{z}_I + \bar{G}_I^\theta \mathbf{w}_I. \tag{48}$$

Therefore, the algebraic equation can be solved by combining Eqs (34) and (35):

$$\mathbf{H}_I\mathbf{u}_I = \mathbf{G}_I\mathbf{t}_I, \tag{49}$$

where

$$\mathbf{H}_I = \begin{bmatrix} \mathbf{H}_I^N & -\overline{\mathbf{H}}_I^\theta \\ \mathbf{0} & \mathbf{H}_I^\theta \end{bmatrix}, \tag{50}$$

$$\mathbf{G}_I = \begin{bmatrix} \mathbf{G}_I^D & \overline{\mathbf{G}}_I^\theta \\ \mathbf{0} & \mathbf{G}_I \end{bmatrix}, \tag{51}$$

$$\mathbf{u}_I = \begin{bmatrix} \mathbf{y}_I \\ \mathbf{v}_I \end{bmatrix}, \tag{52}$$

$$\mathbf{t}_I = \begin{bmatrix} \mathbf{z}_I \\ \mathbf{w}_I \end{bmatrix}, \tag{53}$$

where

$$\hat{\xi}_i' = \frac{\xi_{i+1}+\xi_{i+2}+\cdots\xi_{i+p}}{p}, i = 1,2,\ldots,n-1. \tag{54}$$

5. BEM for design optimization of isogeometric shape

Recall that we can simplify the thermoelasticity problem by not including the heat generator and the body intensity force, thereby revealing the fundamental solution in Eqs (42) and (43).

$$\begin{aligned} &\int_\Gamma T_{ij}(\mathbf{x},\hat{\mathbf{x}})\{u_i(\mathbf{x}) - u_i(\hat{\mathbf{x}})\}d\Gamma - \int_\Gamma \bar{P}_j(\mathbf{x},\hat{\mathbf{x}})\theta(\mathbf{x})d\Gamma \\ &= \int_\Gamma t_i U_{ij}(\mathbf{x},\hat{\mathbf{x}})d\Gamma + \int_\Gamma q_n\bar{Q}_j(\mathbf{x},\hat{\mathbf{x}})d\Gamma, \end{aligned} \tag{55}$$

where

$$\dot{\mathbf{u}} = \mathbf{u}' + \nabla\mathbf{u}^T\mathbf{V}, \tag{56}$$

$$\dot{\mathbf{t}} = \mathbf{t}' + \nabla\mathbf{t}^T\mathbf{V} \tag{57}$$

and

$$\dot{r} = r' + \nabla r^T\mathbf{V}. \tag{58}$$

Now, we can write Eq (55) as

$$\begin{aligned} &\left[\int_\Gamma T_{ij}(\mathbf{x},\hat{\mathbf{x}})\{u_i(\mathbf{x}) - u_i(\hat{\mathbf{x}})\}d\Gamma\right]' - \left[\int_\Gamma \bar{P}_i(\mathbf{x},\hat{\mathbf{x}})\theta(\mathbf{x})d\Gamma\right]' \\ &= \left[\int_\Gamma U_{ij}(\mathbf{x},\hat{\mathbf{x}})t_i(\mathbf{x})d\Gamma\right]' + \left[\int_\Gamma \bar{Q}_i(\mathbf{x},\hat{\mathbf{x}})q_n(\mathbf{x})d\Gamma\right]' \end{aligned} \tag{59}$$

where

$$\begin{aligned}&\left[\int_\Gamma T_{ij}(\mathbf{x},\hat{\mathbf{x}})\{u_i(\mathbf{x})-u_i(\hat{\mathbf{x}})\}d\Gamma\right]'\\&=\int_\Gamma T_{ij}(\mathbf{x},\hat{\mathbf{x}})\{u_i(\mathbf{x})-u_i(\hat{\mathbf{x}})\}V_{k,s}s_k d\Gamma\\&+\int_\Gamma \left[\dot{T}_{ij}(\mathbf{x},\hat{\mathbf{x}})\{u_i(\mathbf{x})-u_i(\hat{\mathbf{x}})\}\right]d\Gamma\\&+\int_\Gamma T_{ij}(\mathbf{x},\hat{\mathbf{x}})\dot{u}_i(\mathbf{x})d\Gamma-\int_\Gamma T_{ij}(\mathbf{x},\hat{\mathbf{x}})\dot{u}_i(\hat{\mathbf{x}})d\Gamma,\end{aligned} \tag{60}$$

$$\begin{aligned}\left[\int_\Gamma \bar{P}_j(\mathbf{x},\hat{\mathbf{x}})\theta(\mathbf{x})d\Gamma\right]' &= \int_\Gamma \left\{\dot{\bar{P}}_j(\mathbf{x},\hat{\mathbf{x}})\theta(\mathbf{x})+\bar{P}_j(\mathbf{x},\hat{\mathbf{x}})\dot{\theta}(\mathbf{x})\right\}d\Gamma\\&+\int_\Gamma \bar{P}_j(\mathbf{x},\hat{\mathbf{x}})\theta(\mathbf{x})V_{k,s}s_k d\Gamma,\end{aligned} \tag{61}$$

$$\left[\int_\Gamma t_i U_{ij}(\mathbf{x},\hat{\mathbf{x}})d\Gamma\right]'=\int_\Gamma \left\{t_i U_{ij}(\mathbf{x},\hat{\mathbf{x}})V_{k,s}s_k+\dot{t}_i U_{ij}(\mathbf{x},\hat{\mathbf{x}})+t_i\dot{U}_{ij}(\mathbf{x},\hat{\mathbf{x}})\right\}d\Gamma, \tag{62}$$

$$\left[\int_\Gamma \bar{Q}_j(\mathbf{x},\hat{\mathbf{x}})q_n(\mathbf{x})d\Gamma\right]'=\int_\Gamma \left\{\dot{q}_n\bar{Q}_j(\mathbf{x},\hat{\mathbf{x}})+q_n\dot{\bar{Q}}_j(\mathbf{x},\hat{\mathbf{x}})+q_n\bar{Q}_j(\mathbf{x},\hat{\mathbf{x}})V_{k,s}s_k\right\}d\Gamma. \tag{63}$$

Appendix and References [40,41] provide more information on the material derivative formulae. Using Eqs (55)–(58), we can rewrite (54) as follows:

$$\begin{aligned}&\int_\Gamma T_{ij}(\mathbf{x},\hat{\mathbf{x}})\{\dot{u}_i(\mathbf{x})-\dot{u}_i(\hat{\mathbf{x}})\}d\Gamma-\int_\Gamma \dot{t}_i U_{ij}(\mathbf{x},\hat{\mathbf{x}})d\Gamma-\int_\Gamma \bar{P}_i(\mathbf{x},\hat{\mathbf{x}})\dot{\theta}(\mathbf{x})d\Gamma-\int_\Gamma \dot{q}_n\bar{Q}_i(\mathbf{x},\hat{\mathbf{x}})d\Gamma\\&=-\int_\Gamma \dot{T}_{ij}(\mathbf{x},\hat{\mathbf{x}})\{u_i(\mathbf{x})-u_i(\hat{\mathbf{x}})\}d\Gamma-\int_\Gamma T_{ij}(\mathbf{x},\hat{\mathbf{x}})\{u_i(\mathbf{x})-u_i(\hat{\mathbf{x}})\}V_{k,s}s_k d\Gamma\\&+\int_\Gamma \dot{\bar{P}}_i(\mathbf{x},\hat{\mathbf{x}})\theta(\mathbf{x})d\Gamma+\int_\Gamma \bar{P}_i(\mathbf{x},\hat{\mathbf{x}})\theta(\mathbf{x})V_{k,s}s_k d\Gamma+\int_\Gamma t_i\dot{U}_{ij}(\mathbf{x},\hat{\mathbf{x}})d\Gamma\\&+\int_\Gamma t_i U_{ij}(\mathbf{x},\hat{\mathbf{x}})V_{k,s}s_k d\Gamma+\int_\Gamma q_n\dot{\bar{Q}}_i(\mathbf{x},\hat{\mathbf{x}})d\Gamma+\int_\Gamma q_n\bar{Q}_i(\mathbf{x},\hat{\mathbf{x}})V_{k,s}s_k d\Gamma.\end{aligned} \tag{64}$$

By using isogeometric discretization, we can write Eqs (59) and (60) in a matrix form as

$$\mathbf{H}_I\dot{\mathbf{u}}_I-\mathbf{G}_I\dot{\mathbf{t}}_I=-\mathbf{H}_I\mathbf{u}_I-\mathbf{H}_I^V\mathbf{u}_I+\dot{\mathbf{G}}_I\mathbf{t}_I+\mathbf{G}_I^V\mathbf{t}_I. \tag{65}$$

6. Design parameterization with h-refinement

The h-refinement technique is used for adding control points by using the following formula:

$$\mathbf{B}_i=(x_i,y_i,z_i;w_i),i=1,\dots,n \tag{66}$$

and its proposed control points are stated as

$$\mathbf{B}_i^w=(w_i x_i,w_i y_i,w_i z_i,w_i). \tag{67}$$

If a new knot $\tilde{\xi}\in[\xi_k,\xi_{k+1})$ is inserted as

$$\tilde{\Xi}=\left\{\xi_1,\xi_2,\dots,\xi_k,\tilde{\xi},\xi_{k+1},\dots,\xi_{n+p},\xi_{n+p+1}\right\}, \tag{68}$$

the position of fresh control points is upgraded by the next equation:

$$\widetilde{\mathbf{B}}_i^w=\alpha_i\mathbf{B}_i^w+(1-\alpha_i)\mathbf{B}_{i-1}^w, \tag{69}$$

where

$$\alpha_i = \begin{cases} 1 & i \le k-p \\ \frac{\tilde{\xi}-\xi_i}{\xi_{i+p}-\xi_i} & k-p+1 \le i \le k. \\ 0 & k+1 \le i \end{cases} \tag{70}$$

7. Numerical results and discussion

The parallelepiped shape radiator for a loop heat pipe (LHP) of a titanium Ti6Al4V as shown in Figure 2 is optimized for space nuclear power system like the one considered in Hartenstine et al. [25], $L = 305$ mm and $h = 26.2$ mm, where two pipes enter the radiator symmetrically and exit after three folds from the same side. Also, the order of basis functions considered in the calculation is $p = 3$.

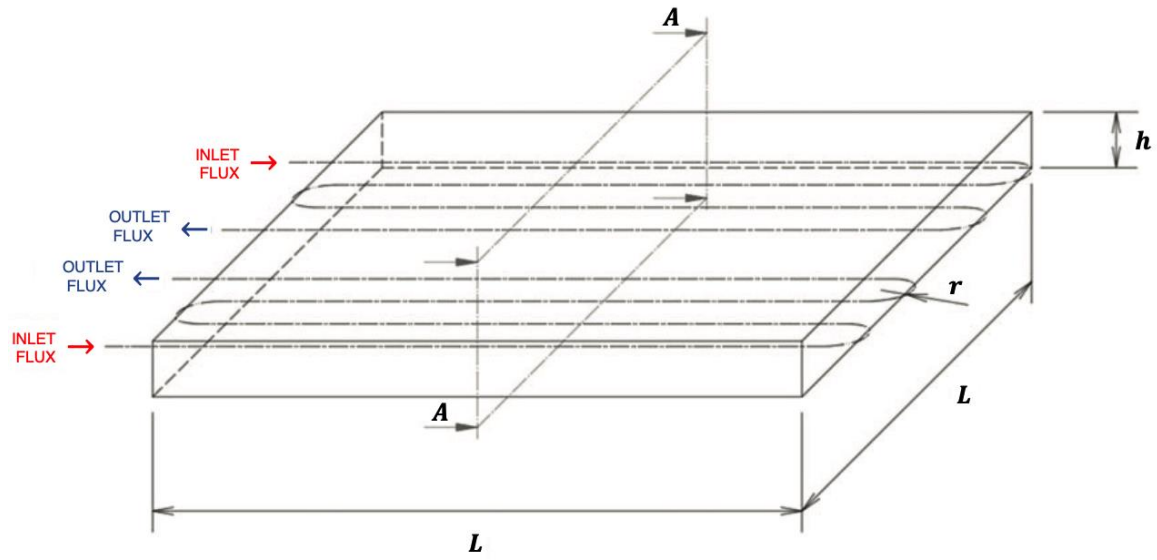

Figure 2. Geometry of the considered radiator model.

We selected a quarter of the cross-section A for the radiator considered model. Thermal boundary conditions made of incoming heat $\boldsymbol{Q}$ on the upper side and fixed temperature θ inside the pipes.

By considering the relationship between the solution of one-temperature heat conduction model (θ) and the solution of three-temperature heat conduction model (θ_α) [14], the 3T distribution θ becomes

$$\theta = \theta_\alpha \text{Summation} - \theta_\alpha \text{Average}$$

where

$$\theta_\alpha \text{Summation} = \theta_e + \theta_i + \theta_r \text{ and } \theta_\alpha \text{Average} = \frac{\theta_e + \theta_i + \theta_r}{3}.$$

Now, we can write the considered optimization problem as follows:
(I) According to the objective function θ based on θ_α subjected to (10)–(12), we obtain the optimal 3T distribution θ as in Figures 3 and 4 below.

(II) According to the objective function $\boldsymbol{u}^*$ subjected to (35)–(37), we obtain the optimal 3T displacement $\boldsymbol{u}$ as in Figures 5 and 6 below.
(III) According to (I) and (II), we can calculate the optimal $3T$ thermal stress σ_{11} as in Figures 7 and 8 below.

The design and nondesign domains must be defined first in the optimization process. In almost all applications, the heat pipes are installed in a sandwich panel with a honeycomb structure at the core. Using the proposed coupled topology optimization algorithm, the honeycomb structure is filled with a single isotropic material for the radiator redesign (design domain). However, the dimensions of the cross section, radiator, and heat pipes remain unchanged. A titanium alloy Ti6Al4V with the thermoelastic properties listed in Table 1 was considered for the redesign and production of the component. It is possible to see that there are eight holes in each section. They are symmetric about both axes of the rectangular section. The radius $R = 9$ mm of the pipe is constant all over the radiator. Each fold has radius $r = 12$, resulting in a distance between the pipes within the domain of $d = 24$ mm.

Table 1. Considered material Ti6Al4V properties.

Material	$\boldsymbol{E}$	$\boldsymbol{\nu}$	$\boldsymbol{\rho}$	$\boldsymbol{k}$	$\boldsymbol{\alpha}$
Ti6Al4V	113.8 GPa	0.342	4430 kg/m^3	6.7 W/mK	9e–6 1/K

Figures 9 and 10 show the effect of rotation on the $\boldsymbol{3T}$ thermal stress $\boldsymbol{\sigma_{11}}$ sensitivity distribution along $\boldsymbol{x}$-axis

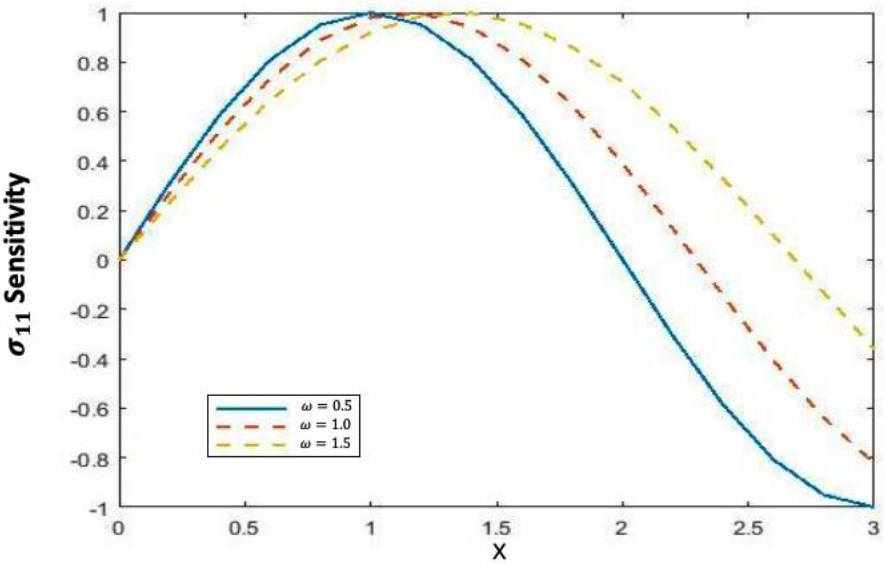

Figure 9. Variation of the $\boldsymbol{3T}$ thermal stress $\boldsymbol{\sigma_{11}}$ sensitivity along $\boldsymbol{x}$-axis in the non-rotating case.

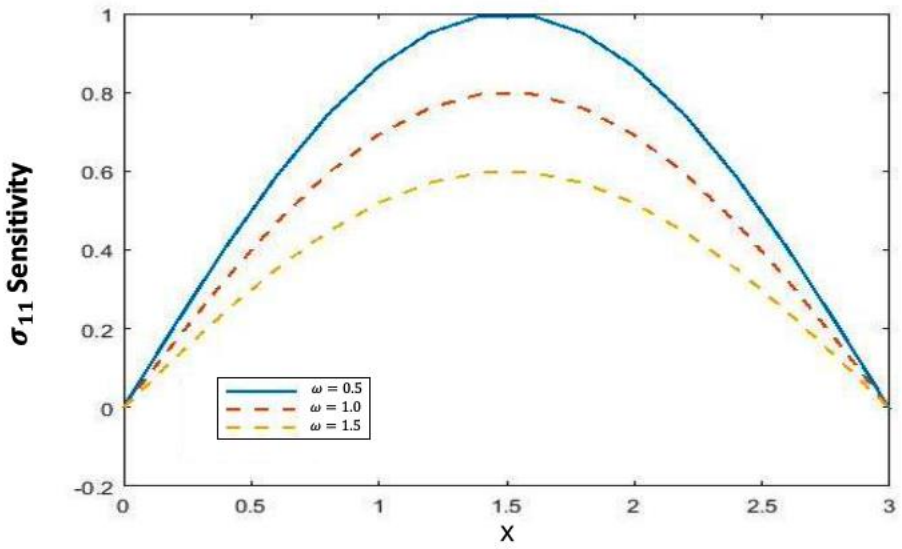

Figure 10. Variation of the $3T$ thermal stress σ_{11} sensitivity along x-axis in the rotating case.

Figures 3 and 4 show the effect of rotation on the optimal 3T distribution θ along x-axis.

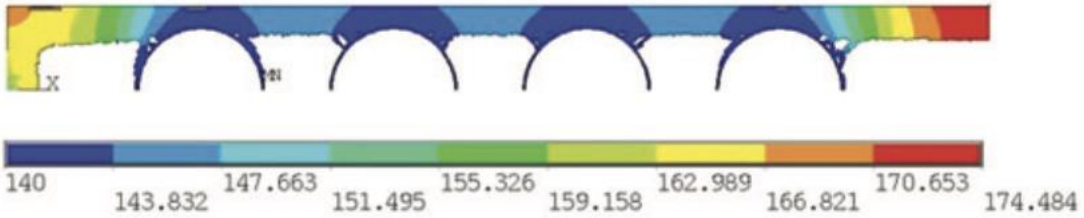

Figure 3. Optimal $3T$ **distribution** θ along x-axis in the non-rotating case.

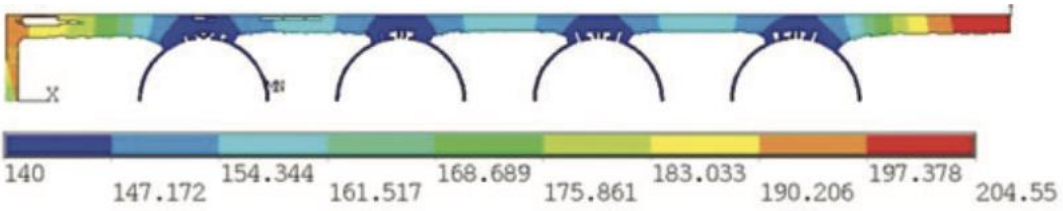

Figure 4. Optimal $3T$ distribution θ along x-axis in the rotating case.

Figures 5 and 6 show the effect of rotation on the optimal displacement u distribution along x-axis.

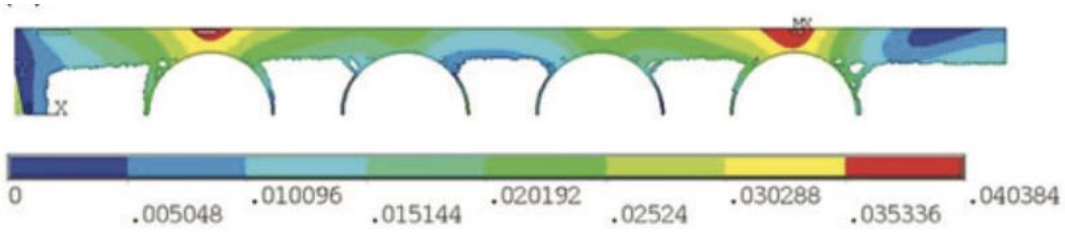

Figure 5. Optimal displacement $\boldsymbol{u}$ distribution along $\boldsymbol{x}$-axis in the non-rotating case.

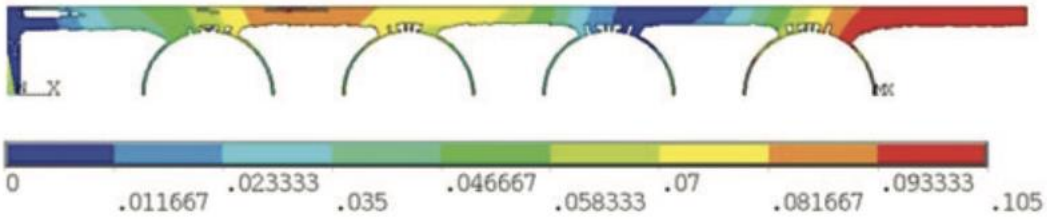

Figure 6. Optimal displacement $\boldsymbol{u}$ distribution along $\boldsymbol{x}$-axis in the rotating case.

Figures 7 and 8 show the effect of rotation on the optimal thermal stress $\boldsymbol{\sigma_{11}}$ distribution along x-axis.

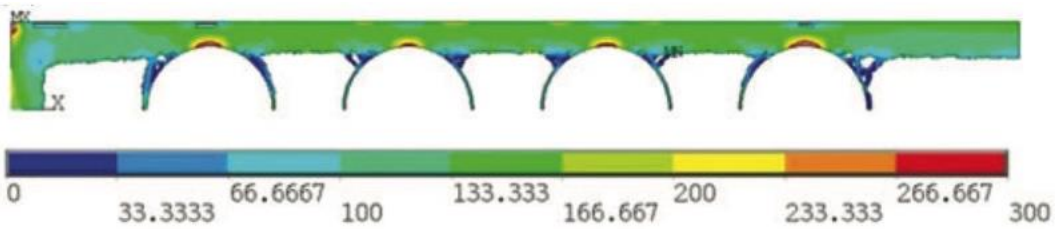

Figure 7. Optimal $\boldsymbol{3T}$ thermal stress $\boldsymbol{\sigma_{11}}$ distribution along $\boldsymbol{x}$-axis in the non-rotating case.

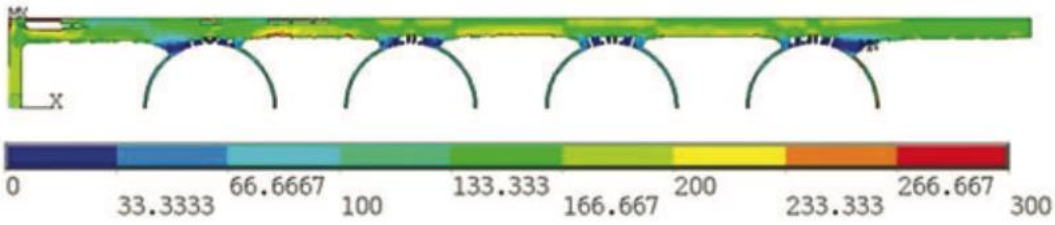

Figure 8. Optimal $\boldsymbol{3T}$ thermal stress $\boldsymbol{\sigma_{11}}$ distribution along $\boldsymbol{x}$-axis in the rotating case.

Figures 11 shows the variations of the special case $\boldsymbol{3T}$ thermal stress sensitivity along $\boldsymbol{x}$-axis for BEM [42–45], lattice Boltzmann method (LBM) of Yin and Zhang [46] and finite element method (FEM) of Soliman and Fahmy [47]. It is clear from this figure that the BEM results of the proposed technique are in excellent agreement with the LBM and FEM, thus confirming the validity and accuracy of our proposed technique.

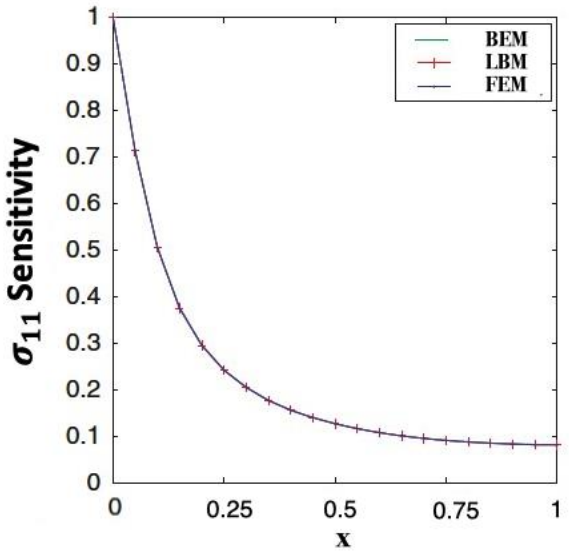

Figure 11. Variation of the $3T$ thermal stress σ_{11} sensitivity along x-axis in the rotating case.

Table 2 shows a comparison of the computer resources needed to perform special case of sensitivity analysis and optimization of rotating three-temperature thermoelastic structures using BEM [42–45], lattice Boltzmann method (LBM) of Yin and Zhang [46] and finite element method (FEM) of Soliman and Fahmy [47]. It can be seen from this table that the proposed BEM is more accurate and efficient than the LBM and FEM.

Table 2. Comparison of computer resources required for BEM, LBM and FEM.

	FEM [47]	**LBM [46]**	**BEM [42-45]**
CPU time (min)	24	20	2
Memory (MB)	22	18	1
Disc space (MB)	34	28	0
Accuracy of results (%)	2.1	1.8	1.1

8. Conclusions

In this study, the isogeometric boundary element method (IGBEM) based on non-uniform rational basis spline (NURBS) is used to perform sensitivity analysis and optimization of rotating three-temperature thermoelastic structures. To include precise geometries and greater continuities, we derive a shape design sensitivity equation within the isogeometric boundary element method formulation. In the considered boundary element technique, the shape design velocity field is divided into normal and tangential components, which has a significant effect on the accuracy of shape design sensitivity. As a result, the developed isogeometric SDSA technique based on the considered boundary element formulation outperforms the traditional DSA method's computational solution. In rotating structures, the isogeometric shape sensitivity and the optimal design for a complex 3T thermoelastic problem are established. The impact of rotation on thermal stress sensitivity, optimal three-temperature, optimal displacement, and optimal thermal stress distributions is investigated. The

SDSA derived from IGBEM is shown to be efficient and applicable for most three-temperature thermoelastic optimization problems.

The accuracy of the proposed method has been confirmed by comparing the obtained results with the lattice Boltzmann method (LBM) results and finite element method (FEM) results. The performance of the proposed method has been confirmed.

Acknowledgments

This research was funded by [Deanship of Scientific Research at Umm Al-Qura University] grant number [22UQU4340548DSR09] And the APC was funded by [Deanship of Scientific Research at Umm Al-Qura University].

The authors would like to thank the Deanship of Scientific Research at Umm Al-Qura University for supporting this work by Grant Code: (22UQU4340548DSR09).

Conflicts of interest

The authors declare no conflicts of interest.

References

1. Y. Tanigawa, Some basic thermoelastic problems for nonhomogeneous structural materials, *Appl. Mech. Rev.*, **48** (1995), 287–300. https://doi.org/10.1115/1.3005103
2. T. J. R. Hughes, J. A. Cottrell, Y. Bazilevs, Isogeometric analysis: CAD, finite elements, NURBS, exact geometry and mesh refinement, *Comput. Methods Appl. Mech. Eng.*, **194** (2005), 4135–4195. https://doi.org/10.1016/j.cma.2004.10.008
3. Y. J. Wang, D. J. Benson, Multi-patch nonsingular isogeometric boundary element analysis in 3D, *Comput. Methods Appl. Mech. Eng.*, **293** (2015), 71–91. https://doi.org/10.1016/j.cma.2015.03.016
4. Y. Bazilevs, V. M. Calo, Y. Zhang, T. J. Hughes, Isogeometric fluid–structure interaction analysis with applications to arterial blood flow, *Comput. Mech.*, **38** (2006), 310–322. https://doi.org/10.1007/s00466-006-0084-3
5. S. Lipton, J. A. Evans, Y. Bazilevs, T. Elguedj, T. J. R. Hughes, Robustness of isogeometric structural discretizations under severe mesh distortion, *Comput. Methods Appl. Mech. Eng.*, **199** (2010), 357–373. https://doi.org/10.1016/j.cma.2009.01.022
6. S. Cho, S. H. Ha, Isogeometric shape design optimization: Exact geometry and enhanced sensitivity, *Struct. Multidisc. Optim.*, **38** (2009), 53–70. https://doi.org/10.1007/s00158-008-0266-z
7. C. Wang, T. Yu, G. Shao, T. T. Nguyen, T. Q. Bui, Shape optimization of structures with cutouts by an efficient approach based on XIGA and chaotic particle swarm optimization, *Eur. J. Mech.-A/Solids*, **74** (2019), 176–187. https://doi.org/10.1016/j.euromechsol.2018.11.009
8. M. Dittmann, M. Franke, I. Temizer, C. Hesch, Isogeometric analysis and thermo- mechanical mortar contact problems, *Comput. Methods Appl. Mech. Eng.*, **274** (2014), 192–212. https://doi.org/10.1016/j.cma.2014.02.012
9. A. H. Taheri, B. Hassani, N. Z. Moghaddam, Thermo-elastic optimization of material distribution of functionally graded structures by an isogeometrical approach, *Int. J. Solids Struct.*, **51** (2014), 416–429. https://doi.org/10.1016/j.ijsolstr.2013.10.014

10. C. Wang, T. Yu, J. L. Curiel-Sosa, N. Xie, T. Q. Bui, Adaptive chaotic particle swarm algorithm for isogeometric multi-objective size optimization of FG plates, *Struct. Multidisc. Optim.*, **60** (2019), 757–778. https://doi.org/10.1007/s00158-019-02238-2
11. A. H. D. Cheng, D. T. Cheng, Heritage and early history of the boundary element method, *Eng. Anal. Bound. Elem.*, **29** (2005), 268–302. https://doi.org/10.1016/j.enganabound.2004.12.001
12. L. Coox, O. Atak, D. Vandepitte, W. Desmet, An isogeometric indirect boundary element method for solving acoustic problems in open-boundary domains, *Comput. Methods Appl. Mech. Eng.*, **316** (2017), 186–208. https://doi.org/10.1016/j.cma.2016.05.039
13. M. A. Fahmy, A novel BEM for modeling and simulation of 3T nonlinear generalized anisotropic micropolar-thermoelasticity theory with memory dependent derivative, *CMES-Comput. Model. Eng. Sci.*, **126** (2021), 175–199. https://doi.org/10.32604/cmes.2021.012218
14. M. A. Fahmy, A new boundary element formulation for modeling and simulation of three-temperature distributions in carbon nanotube fiber reinforced composites with inclusions, *Math. Methods Appl. Sci.*, **1** (2021), 1–16. https://doi.org/10.1002/mma.7312
15. M. A. Fahmy, Boundary element algorithm for nonlinear modeling and simulation of three temperature anisotropic generalized micropolar piezothermoelasticity with memory-dependent derivative, *Int. J. Appl. Mech.*, **12** (2020), 2050027. https://doi.org/10.1142/S1758825120500271
16. M. A. Fahmy, S. Shaw, S. Mondal, A. E. Abouelregal, K. Lotfy, I. A. Kudinov, et al., Boundary element modeling for simulation and optimization of three-temperature anisotropic micropolar magneto-thermoviscoelastic problems in porous smart structures using NURBS and genetic algorithm, *Int. J. Thermophys.*, **42** (2021), 29. https://doi.org/10.1007/s10765-020-02777-7
17. M. A. Fahmy, Boundary element modeling of 3T nonlinear transient magneto-thermoviscoelastic wave propagation problems in anisotropic circular cylindrical shells, *Compos. Struct.*, **277** (2021), 114655. https://doi.org/10.1016/j.compstruct.2021.114655
18. M. A. Fahmy, A computational model for nonlinear biomechanics problems of FGA biological soft tissues, *Appl. Sci.*, **12** (2022), 7174. https://doi.org/10.3390/app12147174
19. M. A. Fahmy, M. O. Alsulami, Boundary element and sensitivity analysis of anisotropic thermoelastic metal and alloy discs with holes, *Materials*, **15** (2022), 1828. https://doi.org/10.3390/ma15051828
20. M. A. Fahmy, 3D boundary element model for ultrasonic wave propagation fractional order boundary value problems of functionally graded anisotropic fiber-reinforced plates, *Fractal Fract.*, **6** (2022), 247. https://doi.org/10.3390/fractalfract6050247
21. M. A. Fahmy, A new BEM modeling algorithm for size-dependent thermopiezoelectric problems in smart nanostructures, *CMC*, **69** (2021), 931–944. https://doi.org/10.32604/cmc.2021.018191
22. M. A. Fahmy, Implicit–explicit time integration DRBEM for generalized magneto-thermoelasticity problems of rotating anisotropic viscoelastic functionally graded solids, *Eng. Anal. Bound. Elem.*, **37** (2013), 107–115. https://doi.org/10.1016/j.enganabound.2012.08.002
23. M. A. Fahmy, Boundary element modeling of fractional nonlinear generalized photothermal stress wave propagation problems in FG anisotropic smart semiconductors, *Eng. Anal. Bound. Elem.*, **134** (2022), 665–679. https://doi.org/10.1016/j.enganabound.2021.11.009
24. M. Yoon, S. Cho, Isogeometric shape design sensitivity analysis of elasticity problems using boundary integral equations, *Eng. Anal. Bound. Elem.*, **66** (2016), 119–128. https://doi.org/10.1016/j.enganabound.2016.01.010

25. W. A. Wall, M. A. Frenzel, C. Cyron, Isogeometric structural shape optimization, *Comput. Methods Appl. Mech. Eng.*, **197** (2008), 2976–2988. https://doi.org/10.1016/j.cma.2008.01.025
26. M. Yoon, M. J. Choi, S. Cho, Isogeometric configuration design optimization of heat conduction problems using boundary integral equation, *Int. J. Heat Mass Tran.*, **89** (2015), 937–949. https://doi.org/10.1016/j.ijheatmasstransfer.2015.05.112
27. B. Chen, L. Tong, Thermomechanically coupled sensitivity analysis and design optimization of functionally graded materials, *Comput. Methods Appl. Mech. Eng.*, **194** (2005), 1891–1911. https://doi.org/10.1016/j.cma.2004.07.005
28. K. Dems, Z. Mroz, Variational approach to sensitivity analysis in thermoelasticity, *J. Therm. Stresses*, **10** (1987), 283–306. https://doi.org/10.1080/01495738708927014
29. D. A. Tortorelli, G. Subramani, S. C. Y. Lu, R. B. Haber, Sensitivity analysis for coupled thermoelastic systems, *Int. J. Solids Struct.*, **27** (1991), 1477–1497. https://doi.org/10.1016/0020-7683(91)90073-O
30. G. J. W. Hou, J. S. Sheen, C. H. Chuang, Shape-sensitivity analysis and design optimization of linear, thermoelastic solids, *AIAA J.*, **30** (1992), 528–537. https://doi.org/10.2514/3.10948
31. Q. Li, G. P. Steven, Y. M. Xie, Thermoelastic topology optimization for problems with varying temperature fields, *J. Therm. Stresses*, **24** (2001), 347–366. https://doi.org/10.1080/01495730151078153
32. B. Y. Lee, B. M. Kwak, Shape optimization of two-dimensional thermoelastic structures using boundary integral equation formulation, *Comput. Struct.*, **41** (1991), 709–722. https://doi.org/10.1016/0045-7949(91)90181-K
33. W. Fang, Z. An, T. Yu, T. Q. Bui, Isogeometric boundary element analysis for two-dimensional thermoelasticity with variable temperature, *Eng. Anal. Bound. Elem.*, **110** (2020), 80–94. https://doi.org/10.1016/j.enganabound.2019.10.003
34. Q. X. Lieu, J. Lee, Modeling and optimization of functionally graded plates under thermo-mechanical load using isogeometric analysis and adaptive hybrid evolutionary firefly algorithm, *Compos. Struct.*, **179** (2017), 89–106. https://doi.org/10.1016/j.compstruct.2017.07.016
35. Z. An, T. Yu, T. Q. Bui, C. Wang, N. A. Trinh, Implementation of isogeometric boundary element method for 2-D steady heat transfer analysis, *Adv. Eng. Softw.*, **116** (2018), 36–49. https://doi.org/10.1016/j.advengsoft.2017.11.008
36. D. F. Rogers, *An introduction to NURBS: With historical perspective*, Elsevier, 2000.
37. L. A. Piegl, W. Tiller, *The NURBS book (Monographs in visual communication)*, 1996.
38. A. Hadjidimos, Successive overrelaxation (SOR) and related methods, *J. Comput. Appl. Math.*, **123** (2000), 177–199. https://doi.org/10.1016/S0377-0427(00)00403-9
39. Y. Liu, T. J. Rudolphi, Some identities for fundamental solutions and their applications to weakly-singular boundary element formulations, *Eng. Anal. Bound. Elem.*, **8** (1991), 301–311. https://doi.org/10.1016/0955-7997(91)90043-S
40. J. C. F. Telles, A self-adaptive co-ordinate transformation for efficient numerical evaluation of general boundary element integrals, *Int. J. Numer. Methods Eng.*, **24** (1987), 959–973. https://doi.org/10.1002/nme.1620240509
41. E. J. Haug, K. K. Choi, V. Komkov, *Design sensitivity analysis of structural systems*, Academic Press, 1986.
42. M. A. Fahmy, Shape design sensitivity and optimization for two-temperature generalized magneto-thermoelastic problems using time-domain DRBEM, *J. Therm. Stresses*, **41** (2018), 119–138. https://doi.org/10.1080/01495739.2017.1387880

43. M. A. Fahmy, Shape design sensitivity and optimization of anisotropic functionally graded smart structures using bicubic B-splines DRBEM, *Eng. Anal. Bound. Elem.*, **87** (2018), 27–35. https://doi.org/10.1016/j.enganabound.2017.11.005
44. M. A. Fahmy, Modeling and optimization of anisotropic viscoelastic porous structures using CQBEM and moving asymptotes algorithm, *Arab. J. Sci. Eng.*, **44** (2019), 1671–1684. https://doi.org/10.1007/s13369-018-3652-x
45. M. A. Fahmy, A new boundary element strategy for modeling and simulation of three temperatures nonlinear generalized micropolar-magneto-thermoelastic wave propagation problems in FGA structures, *Eng. Anal. Bound. Elem.*, **108** (2019), 192–200. https://doi.org/10.1016/j.enganabound.2019.08.006
46. X. Yin, J. Zhang, An improved bounce-back scheme for complex boundary conditions in lattice Boltzmann method, *J. Comput. Phys.*, **231** (2012), 4295–4303. https://doi.org/10.1016/j.jcp.2012.02.014
47. A. H. Soliman, M. A. Fahmy, Range of applying the boundary condition at fluid/porous interface and evaluation of beavers and Joseph's slip coefficient using finite element method, *Computation*, **8** (2020), 14. https://doi.org/10.3390/computation8010014

Appendix

The fundamental solutions material and derivatives are derived, as follows:

$$\dot{\eta}(\mathbf{x},\hat{\mathbf{x}}) = -\frac{1}{\gamma}\frac{1}{2\pi r}\dot{r} = -\frac{1}{\gamma}\frac{1}{2\pi r}r_{,k}\big(V_k(\mathbf{x}) - V_k(\hat{\mathbf{x}})\big), \tag{A1}$$

$$\dot{w}_n(\mathbf{x},\hat{\mathbf{x}}) = \frac{\dot{r}}{2\pi r^2}\frac{\partial r}{\partial n} - \frac{1}{2\pi r}\left(\frac{\partial r}{\partial n}\right) = \frac{1}{2\pi r^2}\frac{\partial}{\partial n}r_{,k}\big(V_k(\mathbf{x}) - V_k(\hat{\mathbf{x}})\big)$$

$$-\frac{1}{2\pi r}\frac{1}{r}\big(\delta_{ik} - r_{,i}r_{,k}\big)\{V_k(\mathbf{x}) - V_k(\hat{\mathbf{x}})\}n_i - \frac{1}{2\pi r}r_{,i}\big(-V_{k,s}n_k\big)s_i, \tag{A2}$$

$$\dot{U}_{ij} = \frac{1}{8\pi\mu(1-v)r}\big\{\delta_{jk}r_i + \delta_{ik}r_{,j} - (3-4v)\delta_{ij}r_{,k} - 2r_i r_{,j}\, r_{,k}\big\}\{V_k(\mathbf{x}) - V_k(\hat{\mathbf{x}})\}, \tag{A3}$$

$$\dot{T}_{ij} = -\frac{(1-2v)}{4\pi(1-v)r^2}\big\{\big(2r_i n_j r_{,k} - \delta_{ik}n_j - \delta_{jk}n_i - \delta_{ij}r_{,k}\, r_{,m}n_m\big)\big\}\{V_k(\mathbf{x}) - V_k(\hat{\mathbf{x}})\}$$
$$-\frac{1}{4\pi(1-v)r^2}\Big\{r(1-2v)\big(\delta_{ij}n_k + 2r_{,i}r_j n_k\big) + 2\frac{\partial r}{\partial n}\big(\delta_{ik}r_j - 3r_{,i}r_{,k}r_j + \delta_{jk}r_i\big)\Big\}\{V_k(\mathbf{x}) - V_k(\hat{\mathbf{x}})\}$$
$$+\frac{(1-2v)}{4\pi(1-v)r}\big(r_{,i}\,V_{l,s}n_l s_j + r_{,j}V_{l,s}n_l s_i\big) - \frac{1}{4\pi(1-v)r}\Big\{r_k V_{l,s}n_l s_k\Big((1-2v)\delta_{ij} + 2r_{,i}\,r_{,j}\Big)\Big\}, \tag{A4}$$

$$\dot{\bar{P}}_l = -\frac{\alpha(1+v)}{4\pi(1-v)}\frac{r_{,k}}{r}\big(V_k(\mathbf{x}) - V_k(\hat{\mathbf{x}})\big) - \frac{\alpha(1+v)}{4\pi(1-v)}\ln\left(\frac{1}{r} - \frac{1}{2}\right)V_{l,s}n_l S_i$$
$$-\frac{\alpha(1+v)}{4\pi(1-v)}\frac{1}{r}\big(\delta_{ik} - r_{,i}r_{,k}\big)(V_k(\mathbf{x}) - V_k(\hat{\mathbf{x}}))\boldsymbol{r}_{,l}n_l$$
$$-\frac{\alpha(1+v)}{4\pi(1-v)}r_{,i}\frac{1}{r}\big(\delta_{lk} - r_{,l}r_{,k}\big)\big(V_k(\mathbf{x}) - V_k(\hat{\mathbf{x}})\big)n_l + \frac{\alpha(1+v)}{4\pi(1-v)}r_{,i}r_{,k}V_{l,s}n_l S_k, \tag{A5}$$

$$\dot{Q}_i = -\frac{(1+v)}{4\pi k(1-v)}\alpha r_{,k}(V_k(\mathbf{x}) - V_k(\hat{\mathbf{x}}))r_{,i}\left[\ln\left(\frac{1}{r}\right) - \frac{1}{2}\right]$$
$$-\frac{(1+v)}{4\pi k(1-v)}\alpha r\frac{1}{r}\left(\delta_{ik} - r_{,i}r_{,k}\right)(V_k(\mathbf{x}) - V_k(\hat{\mathbf{x}}))\left[\ln\left(\frac{1}{r}\right) - \frac{1}{2}\right]$$
$$+\frac{(1+v)}{4\pi k(1-v)}\alpha r r_{,i}\frac{r_{,k}}{r}(V_k(\mathbf{x}) - V_k(\hat{\mathbf{x}})). \quad \text{(A6)}$$